Critical Level Reflection and the Resonant Growth of Nonlinear Mountain Waves

T. L. CLARK

National Center for Atmospheric Research,[1] Boulder, CO 80307

W. R. PELTIER

Department of Physics, University of Toronto, Toronto, Ontario, Canada M5S 1A7

(Manuscript received 26 March 1984, in final form 9 July 1984)

ABSTRACT

We examine the evolution of a field of internal waves launched by stratified flow over symmetric topography in mean flows which reverse direction at some height above the surface. With the gradient Richardson number at this "critical level" in the undisturbed flow restricted to values greater than 0.25, the nonlinear interaction in the region is such that the surface strongly reflects large amplitude internal waves incident upon it. When the critical level is located near certain discrete heights above the ground the incident and reflected waves interfere constructively and the wave amplitude in the low levels is resonantly enhanced by a large factor. These results are related to our previous analyses of the process by which breaking internal waves are able to induce intense downslope windstorms.

1. Introduction

It is well-known that a plane parallel internal wave propagating through a stratified parallel flow is markedly affected at a "critical level" where its intrinsic frequency is Doppler shifted to zero. Miles (1961) provided the basis for the mathematical analysis necessary to demonstrate that a small amplitude internal wave would be completely absorbed at a critical level provided that the local gradient Richardson number was sufficiently in excess of the same critical value of 0.25 which governs the temporal stability of the background flow. Booker and Bretherton (1967) applied Miles' linear analysis to the special case of standing internal waves launched by stratified flow over topography, the same physical problem as will concern us here. When the local Richardson number at the critical level is less than 0.25 and dynamical instability is possible, incident internal waves are "over-reflected" since the interaction is such that the wave actually extracts energy and momentum from the mean flow in the course of the reflection process. Davis and Peltier (1976, 1977, 1979) have analyzed this mechanism in detail and suggested that it may be responsible for certain multilayered turbulent structures which develop on occasion in the nocturnal planetary boundary layer during conditions supportive of shear instability.

These central results of linear theory, that $\mathrm{Ri} > \frac{1}{4}$ implies wave absorption and $\mathrm{Ri} < \frac{1}{4}$ implies wave over-reflection at a critical level, are results which are not liable to remain valid as the wave-induced flow in the vicinity of the critical level develops and nonlinear processes become increasingly important. This fact is well understood in the context of the corresponding problem of barotropic Rossby wave propagation and barotropic instability. Warn and Warn (1978) have clearly shown that a barotropic Rossby wave incident on a critical level is eventually strongly reflected under circumstances in which linear theory predicts the mean state to be barotropically stable. Although the detailed characteristics of the critical layer for internal waves and barotropic Rossby waves are quite different, we might nevertheless expect them to behave similarly in this respect.

Our motivation for the calculations to be described in this paper, which concern the interaction of a spatially localized and topographically forced packet of internal waves with the mean flow at a critical layer, derives from results which we have previously obtained from a series of studies of a related problem. The previous calculations (Clark and Peltier, 1977; Peltier and Clark, 1979, 1980, 1983) were also concerned with topographically forced internal waves, but did not include circumstances in which the mean flow reversed direction and a critical layer exists. The main results established by this previous work is that when the forced internal wave has such large amplitude that it "breaks," in the sense that streamlines (isentropes) locally overturn, then the wave amplitude

[1] The National Center for Atmospheric Research is sponsored by the National Science Foundation.

in the underlying region is subsequently amplified to an intensity which is enormously in excess of that which would be predicted by Long's (1953) model. Although Long's model correctly incorporates the full nonlinear effect of the lower boundary condition it is based upon the assumption of steady state behavior. Our results have therefore established that when the internal wave is forced to exceed critical steepness then a new transient process is triggered which leads to a large increase of wave amplitude in the low levels. The analyses to be reported in this paper are intended to further clarify the nature of this new process.

In previous discussions of the numerically observed amplification of the wave subsequent to breaking, we suggested (e.g., Peltier and Clark, 1979) the possibility that as streamlines locally overturn, the level of breaking begins to appear as a critical level to the wave which is incident upon it from below. This is a reasonable suggestion because the wave deformed mean state into which the additional disturbance propagates is one in which the local horizontal velocity actually does reverse direction. Also, since the local temperature gradient changes from sub- to super-adiabatic as streamlines overturn, the local gradient Richardson number changes discontinuously from a value near $+\frac{1}{2}$ to a value near $-\frac{1}{2}$. Precisely how a nonlinear wave will evolve in time, as this critical condition (of streamline overturning) is exceeded, is therefore unclear although the evolution may well be influenced both by interaction of the wave propagating upwards into the wave-induced region of static instability and by the local convective overturning in the critical region itself. However, if there were substantial reflection from the level of wave breaking and if this reflection were coherent so that the incident and reflected waves interfered constructively, then the possibility clearly exists that the wavefield in the low levels might amplify resonantly. In Peltier and Clark (1983) a simple linear theory of this resonant amplification process was constructed and shown to provide a plausible interpretation of the numerical data.

The basic assumption in this simple theory is that the reflection from the "wave-induced critical layer" (the level of breaking) is inphase with the incident wave, since it is only under this condition that resonant growth is possible. If this assumption is correct then it implies that the nonlinear mountain wave is in a sense "self-tuned" since the height at which wave breaking occurs for symmetric topography is always $3\lambda_z/4$ above the surface (Peltier and Clark, 1979), where λ_z is the vertical hydrostatic wavelength of the wave, and since whenever wave breaking occurs in the slowly varying mean flows which we have analysed the wave always amplifies in the region between this level and the ground. The question which then arises is whether this special height is the only one for which the incident and reflected waves interfere constructively. The calculations to be reported here are intended as a direct test of this fundamental assumption in the resonance hypothesis. We will show by explicit computation of the evolution of the mountain wave field in mean flows with critical layers that only if the height of the reflecting critical layer above the topography is $3\lambda_z/4$ or some integral number of vertical wavelengths in excess of this, will the direct and reflected waves interfere constructively to support a large amplitude resonant response. The analyses therefore fully confirm our original hypothesis as to the physical process which underlies the numerically observed wave amplification obtained in previous work on the mechanism of severe downslope windstorm formation (Peltier and Clark, 1979, 1983).

The paper is organized as follows. Section 2 contains a very brief summary of the characteristics of the numerical model and a succinct review of the most important previous results on the amplification of breaking internal waves. Section 3 briefly describes the physical features of the new critical level calculations and the results of these calculations are presented in Section 4. Section 5 contains a discussion of the implications of these results and some concluding remarks.

2. Features of the numerical model and a summary of previous results on breaking waves

A detailed description of the numerical model which we have been employing in all of our work in nonlinear mountain waves can be found in Clark (1977). Modification of this general mesoscale model necessary for the wave dynamics calculations have been discussed in Clark and Peltier (1977) and other papers referenced previously. The model is anelastic and therefore based on the following approximation to the continuity equation:

$$\nabla \cdot (\bar{\rho}\mathbf{u}) = 0, \tag{1}$$

in which $\bar{\rho}(z)$ is the initial (hydrostatic) background density profile. This approximation suffices to eliminate sound waves entirely as a possible physical process in the hydrostatic system. The relations for conservation of momentum and energy in this system are, respectively,

$$\bar{\rho}\frac{d\mathbf{u}}{dt} = -\nabla p' + \nabla \cdot \tau + \rho'\mathbf{g}, \tag{2}$$

$$\bar{\rho}\frac{d\theta}{dt} = \nabla \cdot \mathbf{H}, \tag{3}$$

where the stress tensor τ and the heat flux vector $\mathbf{H}$ are given by

$$\tau_{ij} = \bar{\rho}K_m D_{ij}, \tag{4}$$

$$H_i = \bar{\rho}K_h \partial_i \theta \tag{5}$$

and the deformation tensor D_{ij} by

$$D_{ij} = \partial_j u_i + \partial_i u_j - 2\partial_i u_i/3. \quad (6)$$

Here $\mathbf{u}$ is the velocity vector, p' and ρ' the pressure and density perturbations, θ the potential temperature and K_m and K_h the eddy diffusivities for momentum and heat. The density perturbation is obtained from the ideal gas law as $\rho' = -\bar{\rho}\theta'/\bar{\theta} + p'/c^2$ where c^2 is the square of the adiabatic sound speed in the hydrostatic background state $\bar{\rho}$, $\bar{p}$, $\bar{\theta}$. The two diffusivities are usually taken equal so that the eddy Prandtl number is unity and their local values are determined through a first order closure as:

$$K_m = (k\Delta)^2|\mathrm{Def}|(1 - \mathrm{Ri})^{1/2}, \quad \mathrm{Ri} \leqslant 0 \quad (7)$$

where, for a two-dimensional model

$$|\mathrm{Def}|^2 = \frac{1}{2}(D_{11}^2 + D_{22}^2) + D_{12}^2. \quad (8)$$

The parameter $\Delta = (\Delta x \cdot \Delta z)^{1/2}$ is the grid resolution where Δx and Δz are the grid spacings in the horizontal and vertical directions and k is a numerical constant (see Lilly, 1962). The Richardson number employed in the turbulence parameterization in (7) is

$$\mathrm{Ri} = g\frac{d\ln\theta/dz}{(\mathrm{Def})^2}. \quad (9)$$

The final crucial ingredient of the numerical model is the method employed to introduce the topography. We employ a tensor transformation to map the domain with bottom topography $z_s(x)$ in two spatial dimensions into a regular parallelepiped. If the original coordinates are (x, z), the new coordinates $(\bar{x}, \bar{z})$ are defined as

$$\bar{x} = x$$

$$\bar{z} = H\frac{[z - z_s(x)]}{[H - z_s(x)]}, \quad (10)$$

where H is the physical height of the numerical model.

The other boundaries of this limited area model also require special consideration. The top boundary is important because internal waves incident upon it from below will be perfectly reflected and contaminate the integration unless care is taken. Although some success has recently been obtained for steady state internal wave problems using the local radiation boundary condition method implemented by Béland and Warn (1975) (e.g., see Klemp and Duran, 1983) we have continued to employ a layer near the upper boundary in which the viscosity rises smoothly to a large value in order to effect the absorption necessary to ensure that the integration in the lower levels remains uncontaminated by reflected disturbances. Although this method is wasteful of storage it is efficient at preventing these undesirable reflections. The lateral boundaries are treated using a variant of the method of extrapolation discussed by Orlanski (1976). The computational domain is illustrated schematically in Fig. 1. Before proceeding to describe the new critical layer experiments which we have performed with this model we will provide in what follows a very brief summary of the previous results which have motivated this new work.

Severe downslope windstorm simulations and observations suggest the development of regions of convective overturning which are produced by the strong surface forcing of internal waves. Although the observations are not of sufficient detail to either substantiate or refute the existence of regions of overturning streamlines (e.g., Lilly and Klemp, 1980) all of the recent numerical simulations have produced such a result (e.g., Peltier and Clark, 1979; Klemp and Duran, 1983; Clark and Farley, 1984). Similarly, for the case of waves impinging on a critical layer with parameters representative of atmospheric conditions, one expects the nonlinear terms to lead to regions of overturning flow providing the waves are of sufficient amplitude. Implicit in this discussion is the assumption that the nonlinear terms dominate over the effects of local dissipation in the convectively unstable region. If, for example, the dissipation was sufficiently strong to maintain the local Richardson number at values exceeding 0.25, then instead of wave reflection one would expect primarily wave energy absorption and dissipation. Laboratory experiments such as those of Koop (1981) appear to fall in this latter category but due to the very large values

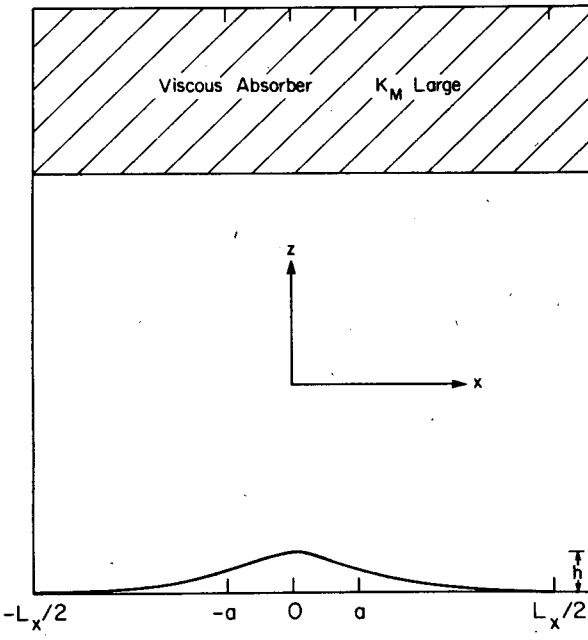

FIG. 1. Schematic illustration of the computational domain in which the equations of the numerical model are integrated.

of the gradient Richardson number (≥ 150) and mean shears ($\sim 0.5\ s^{-1}$) his results are of questionable applicability to the conditions more typical of nature which are considered in this paper. As discussed by Koop (1981), his parameters fall in the range in which the long time behavior is strongly influenced by viscous effects. For example, the ratio of $t_{NL}/t_\nu \sim O(1)$ where t_{NL} is the time scale at which nonlinear effects become important and t_ν is the time scale at which dissipation dominates. The critical layer calculations of this paper have values of $t_{NL}/t_\nu \sim O(10^{-3})$ which clearly indicates the long time importance of the nonlinear terms. Clark and Farley (1984) have shown with their three-dimensional simulations of a severe downslope windstorm case that realistic direct simulation of turbulence in the convectively unstable wave breaking region leads to convective overturning and a realistic simulation of regions of intense turbulence as obtained from the aircraft observations of Lilly and Zipser (1972). This work supports the notion that the nonlinear effects play a dominant role in the wave breaking region.

Figure 2 shows vertical Reynolds stress profiles through a field of standing internal waves in a mean flow with constant Brunt–Väisälä frequency $N = 0.99 \times 10^{-2}\ s^{-1}$ ($N^2 = gd\ \ln\theta/dz$) and wind speed $U = 4\ m\ s^{-1}$. The Reynolds stress is defined by the correlation

$$\mathrm{Re}(z) = \langle \rho_0 u' w' \rangle, \tag{11}$$

where the angle brackets denote integration in the horizontal x-direction. Graphical depictions of the field of internal waves itself are provided by Peltier and Clark (1983). The topographic forcing employed in the calculations which produced these stress profiles was bell shaped with $z_s(x) = ha^2/(x^2 + a^2)$ where the maximum height is $h = 400$ m and the topographic half width is $a = 3$ km. Vertical profiles Re(z) are drawn for two different sets of numerical calculations in plates (a) and (b) with individual profiles drawn at 10 minute intervals beginning at time $t = 230$ minutes from the start of the run. Plate (a), which is for an experiment numbered 34, shows the output from a simulation which employed 97 vertical levels while Plate (b) shows results for the same physical situation but using a model with 192 vertical levels. Further numerical details will be found in Peltier and Clark (1983).

These flows were both established by first computing the steady state wavefield forced by a uniform mean flow of speed 5 m s^{-1} and then decelerating this mean flow to the final speed of 4 m s^{-1}. The history of the surface wave drag $D_w(0)$ defined as

$$D_w(0) = +\int_{-\infty}^{+\infty} z_s(x) \frac{\partial p}{\partial x}\, dx \tag{12}$$

for these two integrations is shown in Fig. (3). This is just the force that the fluid exerts on the boundary as a consequence of the downstream pressure drop which is established by the process of wave generation. This must of course equal Re(0) and comparison of the results in Figs. (2) and (3) shows that this required balance is met by our numerical fields. Inspection of the drag histories shown in Fig. 3 reveals that, following the period of mean flow deceleration from a speed of 5 to a speed of 4 m s^{-1}, the surface wave drag rises approximately linearly with time from a

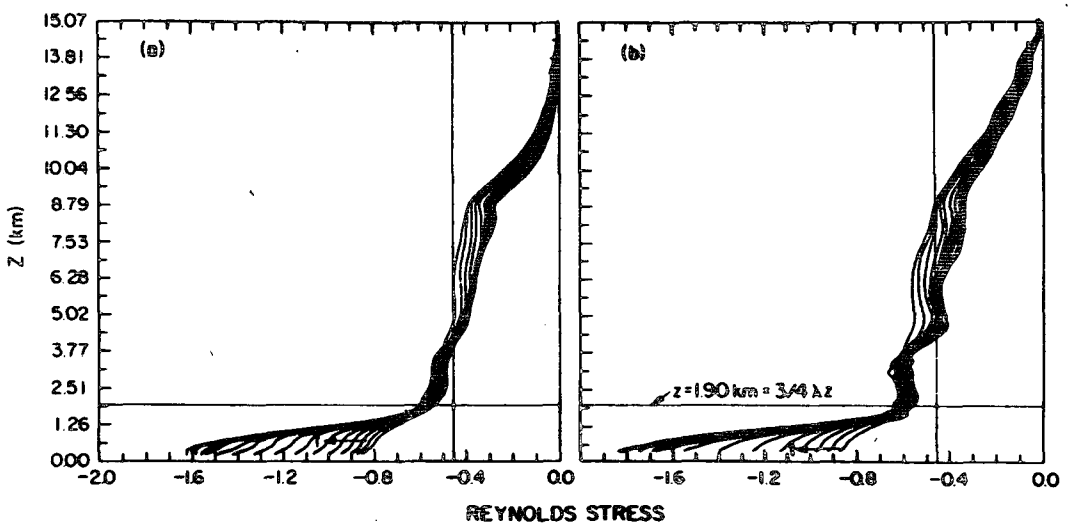

FIG. 2. Reynolds stress profiles through the field of standing waves. The results in plate (a) are from a model with 97 vertical levels while those in plate (b) are from a model with 192 vertical levels but otherwise identical to that which produced the results in plate (a). The height $z = 3\lambda_z/4$ at which the standing waves break is marked on each plate.

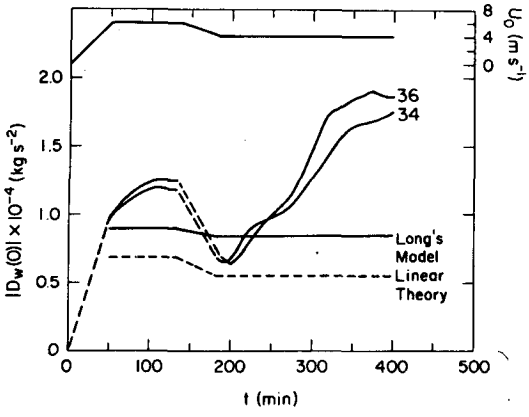

FIG. 3. Surface wave drag as a function of time for the two integrations numbered 34 and 36 which produced the Reynolds stress profiles shown in plates (a) and (b) of Fig. 2 respectively. The time variation of the strength of the mean flow is shown at the top of the figure. Following the time of deceleration from 5 to 4 m s^{-1} the surface wave drag rises rapidly.

value near 0.6×10^4 kg s^{-2} to a value near 2×10^4 kg s^{-2} over a timescale of approximately 200 minutes. The importance of this result is that Long's model predicts that the surface wave drag should *decrease* rather than increase when the mean flow speed is decreased from 5 to 4 m s^{-1}. The drag predicted by Long's model is also shown on the figure. It is important to note that not only does the wave drag increase upon mean flow deceleration but also that the factor by which the drag increases is in excess of 3; that is, the eventual drag in the nonlinearly equilibrated state is several hundred percent greater than predicted by a steady state nonlinear calculation.

In order to understand the mechanism which supports this drag amplification we need first to note that, when the mean flow speed is decreased from 5 to 4 m s^{-1}, the Froude number Fr = Nh/U increases from 0.7924 to 0.9905. Analysis by Miles and Huppert (1969) shows that, for the combination of mean flow and topography which we are employing here, internal waves break when Fr > 0.85. Thus deceleration of the mean flow from 5 to 4 m s^{-1} induces wave breaking, and according to our numerical results when streamlines are forced to overturn the flow becomes strongly time dependent, and surface drag increases precipitously.

The nature of the process which supports the drag amplification is suggested by inspection of the stress profiles in Fig. 2. As the surface drag begins to amplify following the period of mean flow deceleration at t = 200 minutes the stress profile becomes strongly divergent in the layer between the ground and the height $z = 3\lambda_z/4$ which is marked on the figure. Peltier and Clark (1979) showed that this is precisely the height at which streamlines first overturn. Above this height the momentum flux in the wavefield remains constant and nondivergent except in the layer above z = 8.79 km in which viscous absorption has been enhanced to prevent wave reflection from the upper lid of the numerical domain. The thin vertical lines on both plates (a) and (b) of Fig. 2 are drawn for the stress Re = -0.45×10^4 kg s^{-2} which is precisely the stress predicted by Long's model for a wave of critical amplitude in which the streamline through the height $z = 3\lambda_z/4$ has an exactly vertical orientation.

The implications of these calculations, which are discussed at considerably greater length by Peltier and Clark (1983), should be quite clear. When the internal wave is forced to exceed critical steepness, an equilibration appears to occur at the level of breaking which is such that the amplitude of the wave transmitted through this level is restricted to remain equal to that associated with precisely vertical streamlines at the critical height. The forced disturbance which is in excess of that required to maintain critical steepness is apparently reflected from this level, as evidenced by the continuous growth of wave amplitude in the cavity between $z = 3\lambda_z/4$ and the ground. As pointed out before, this growth is very nearly linear in time and is fully explicable in terms of the very simple theory outlined by Peltier and Clark (1983). This theory shows that if the reflection from the critical height is in phase with the incident wave, then the superposed disturbance amplifies in time like a classical harmonic oscillator which is forced at its resonance frequency; this growth *is* of course linear in time.

The new numerical experiments to be described in the following sections have been designed specifically to investigate the validity of the assumptions upon which this simple theory is based. What we will do is use the fact that the nonlinear interaction between a packet of internal waves and the mean flow in a critical layer is such that reflection of the incident wave does eventually occur. By varying the height of the critical layer above the ground we will be able to arbitrarily fix the length scale of the cavity in which a wave of fixed frequency and vertical wavelength exists. Our resonance hypothesis for the interpretation of the data shown in Figs. 2 and 3 will clearly be verified if we can show that resonant growth of the disturbance in the cavity between the level of mean flow reversal and the ground occurs only if the height of the critical layer is $z = 3\lambda_z/4$ or some integral number of vertical wavelengths in excess of this.

3. Parameter settings for the family of critical layer experiments

All of the new calculations which we will report here have been carried out using a model with 202 grid points in the horizontal and 162 grid points in the vertical. The grid dimensions have been fixed at Δx = 400 m and Δz = 50 m and the time step in

all integrations is $\Delta t = 5$ s. We will discuss the nature of the internal wave response is mean flows with the properties

$$N = 0.02\ \text{s}^{-1}, \tag{13a}$$

$$U(z) = U_0 \tanh[(z - z_i)/b]. \tag{13b}$$

In (13b) b is the half-width of the shear layer through which the strength of the mean flow changes from $-U_0$ in the low levels to $+U_0$ in the upper levels and z_i is the height of the inflection point in the wind profile at which the mean flow reverses direction. For all of these new calculations the two former parameters will be held fixed at the values

$$b = 600\ \text{m}, \tag{13c}$$

$$U_0 = 8\ \text{m s}^{-1}. \tag{13d}$$

Since the gradient Richardson number $\text{Ri} = N^2/(dU/dz)^2$ it is clear that its minimum value in the mean flow (13a,b) occurs at the inflection point $z = z_i$ where

$$\text{Ri}_{\min} = \frac{N^2}{(U_0/b)^2} = 2.25 \tag{14}$$

so that the undisturbed flow is stable against the onset of shear instability and linear theory predicts that a plane internal wave with zero phase velocity whose critical level is also at $z = z_i$ will be quite strongly absorbed.

The topographic forcing to be employed in these new calculations will again be the bell shaped topography

$$z_s(x) = \frac{a^2 h}{x^2 + a^2} \tag{15}$$

and we will fix a and h for all simulations at the values

$$h = 300\ \text{m}, \tag{16a}$$

$$a = 3\ \text{km}. \tag{16b}$$

In combination with (13) this implies a Froude number for the flow in the low levels of

$$\text{Fr} = \frac{Nh}{U_0} = 0.75 \tag{17}$$

which is less than the critical value of 0.85 above which the forced internal waves would be expected to break if the mean flow speed were equal to U_0 at all heights. It is important to note however that Fr is sufficiently close to this critical value that wavebreaking may be induced readily by the decrease of windspeed in the critical layer region. The Froude number is just 2π times the ratio of the maximum height of the topography to the vertical hydrostatic wavelength of the forced internal waves. It is also important to note that because $Nh/U_0 < 1$ in the low levels we do not expect any significant upstream blocking of the incident stream to occur. This is important insofar as boundary conditions at the upstream boundary are concerned which would be difficult to implement otherwise.

The only remaining parameter which we have yet to specify to complete the characterization of the basic state is the height z_i of the level at which the mean wind reverses direction and which is the critical level for the spatially stationary internal waves forced by the topography. The results which we will proceed to report are for a sequence of 12 very long time integrations of the model equations in which this is the sole parameter which is altered between experiments. For obvious reasons we choose to specify this critical level height in units of the vertical hydrostatic wavelength of the internal waves which is $\lambda_z = 2\pi U_0/N = 2.513$ km on the asymptote of the hyperbolic tangent mean state wind profile. Although the local vertical wavelength clearly changes rapidly as the wave approaches the critical height itself and the vertical component of the group velocity tends to zero (Booker and Bretherton, 1967) the asymptotic wavelength does turn out to be the length scale in terms of which the final results scale naturally. It may also be significant to note that the half-width of the shear layer $b = 600$ m is very nearly $\lambda_z/4$, and so the mean state critical layer has been scaled as closely as possible to the wave induced critical layer of the last section.

The point of these experiments is that by raising or lowering the height at which the wind reversal occurs we will be able to increase or decrease the height of critical level reflection. Since the wave is in fact forced to break as it propagates towards the height at which $U = 0$ we can force wave breaking to occur in these models at an arbitrary distance above the ground. The question which we wish to answer is whether the amplitude of the response in the region beneath the critical level is a strong function of z_i/λ_z, as we would expect of a system capable of resonance. If we discover resonant amplification for $z_i = 3\lambda_z/4 + n\lambda_z$, where n is an integer but significantly weaker response away from this condition then we will have established the validity of the self-response hypothesis advanced to explain the breaking wave simulations discussed in the last section.

4. Results of the numerical simulations

Figure 4 shows surface wave drag histories for the 12 separate long time integrations of the model for values of z_i/λ_z varying from 0.75 to 1.85. In each integration the model is initialized by setting the velocity field equal to that determined by a streamfunction Ψ satisfying $\nabla^2\Psi = \omega_0$ where ω_0 is the vorticity of the undisturbed parallel flow. This clearly yields a potential flow when the background windfield is uniform and $\omega_0 = 0$. The initial potential temperature field is taken equal to the constant stability

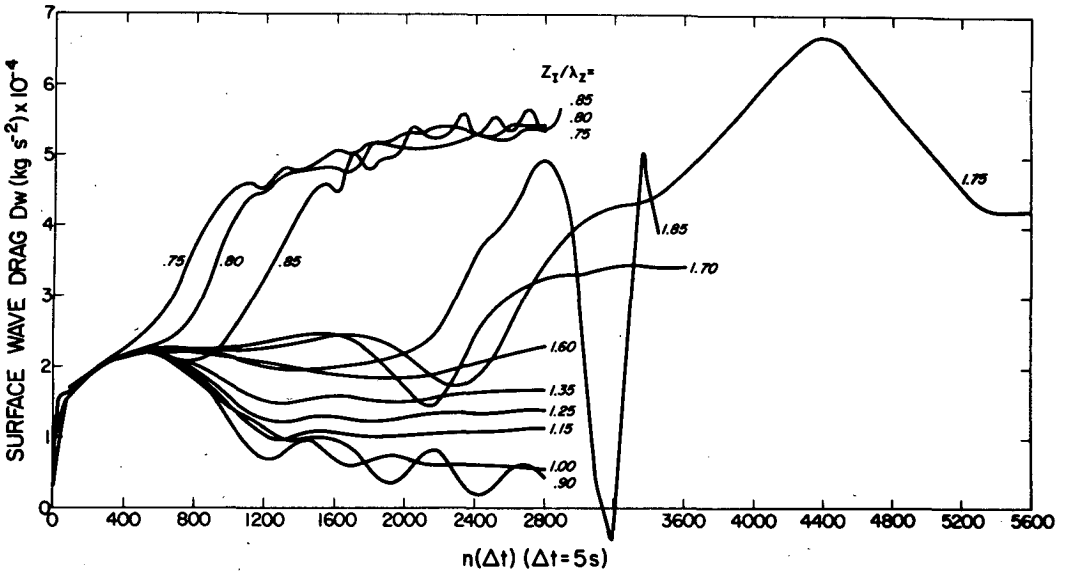

FIG. 4. Surface wave drag histories for each of the 12 long-time integrations of the model equations for mean flows which reverse direction at some height above the ground. The nondimensional height of the critical level z_i/λ_z is marked adjacent to each curve. Note the precipitous decrease of surface drag which occurs when z_i/λ_z is increased from 0.85 to 0.9 and the recovery which occurs upon further increase of this parameter.

background variation $\bar{\theta}(z)$. This initialization enforces a sufficiently smooth startup that severe contamination of the integrations by initial transients does not occur. It is important to note that in this more efficient initialization the initial buoyancy field is zero which ensures that the initial tendency of the vorticity also vanishes.

Inspection of the individual drag histories in Fig. 4 shows that the surface drag is indeed a very strong function of the critical level height z_i/λ_z. For $z_i/\lambda_z = 0.75$ the surface drag continues to grow rapidly following the startup phase of the simulation, eventually saturating near $D_w(0) = 5.5 \times 10^4$ kg s^{-2}. The integrations for $z_i/\lambda_z = 0.8$ and 0.85 also saturate near the same value although in each of these cases the rise to maximum amplitude is further delayed in time as z_i/λ_z increases.

When z_i/λ_z is increased further from 0.85 to 0.9 a marked change in the drag curve takes place. Rather than continuing to rise following the startup phase the drag now decreases rapidly and in a highly oscillatory fashion to eventually reach an equilibrium by $t = 2800\Delta t$ which is *an order of magnitude lower* than the surface drag which occurred at $z_i/\lambda_z = 0.85$. The increase in critical level height required to effect this enormous drag reduction is only of order 6%. As the parameter z_i/λ_z further increases from 0.9 to 1.0, 1.15, 1.25, 1.35, and 1.6 the drag curve saturates at successively higher values but these are still a factor of 2 or 3 below the level reached by the flows with $z_i/\lambda_z = 0.75$, 0.8, or 0.85. A further transition takes place as z_i/λ_z increases above $z_i/\lambda_z = 1.6$.

The drag history for the flow with $z_i/\lambda_z = 1.7$ is fairly flat following startup to a time near $1600\Delta t$ after which it falls and then rises to saturate at a somewhat higher level. This same characteristic initial time dependence of the drag history also occurs when $z_i/\lambda_z = 1.75$ although in this case the drag continues to increase until it eventually saturates (with strong time dependence) at a level very near that achieved by the flows with $z_i/\lambda_z = 0.75$, 0.80, and 0.85. The change in slope of the drag history for the flow with $z_i/\lambda_z = 1.75$ near $t = 3500\Delta t$ is coincident with the time at which the internal wave breaks beneath the mean flow critical level at $z = 3\lambda_z/4$, so that the development of this flow is a rather complex one which includes elements peculiar to flows of the type discussed in Section 2 of this paper as well as the pure critical level interaction which appears to have been isolated for flows with $z_i/\lambda_z \leq 1.7$. The drag history for the simulation at $z_i/\lambda_z = 1.85$ is again characterized by a sharp rise to very high values although in this case the curve peaks more rapidly and exhibits intense time dependence thereafter.

The intense time dependence in this $z_i/\lambda_z = 1.85$ case is attributed to an interaction between the two levels of maximum stream line steepening, i.e., $z_i/\lambda_z = 0.75$ and 1.75. It is not surprising that the interaction takes a considerably different form for a case where $z_i/\lambda_z > 1.75$ than for a case where $z_i/\lambda_z \leq 1.75$ because it is only when $z_i > 1.75$ that we have two levels of maximum stream line steepening below the critical level. Thus the effects of surface wave launching, wave-induced resonance and critical level reflec-

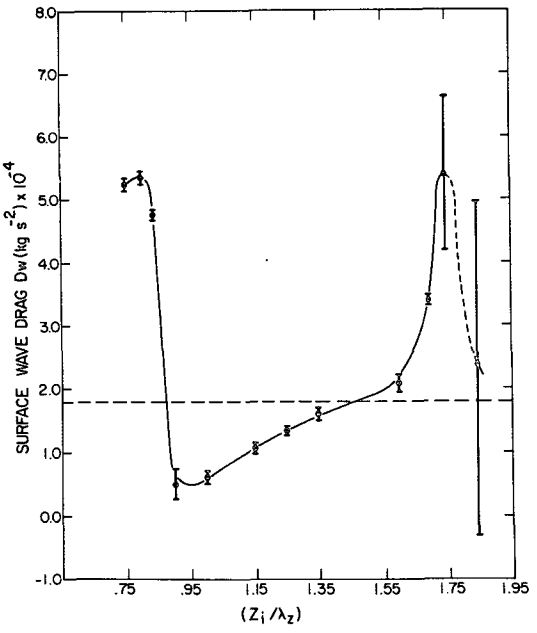

FIG. 5. Eventual "steady state" surface drag as a function of the nondimensional distance of the critical level above the ground z_i/λ_z. Note the resonant peaks centered on $z_i/\lambda_z = 0.75$ and $z_i/\lambda_z = 1.75$. The drag which would be predicted by Long's model for a height independent mean flow of speed equal to that on the lower asymptote of the hyperbolic tangent wind profile is shown as the dashed line.

tion give a strongly assymmetrical type of response for finite variations of z_i from the resonant peak value of $z_i/\lambda_z = 1.75$. Instead of a long time adjustment to the critical level reflection, surface wave forcing and a *single* level of self-induced wave resonance (which is itself quite variable in time) for the $z_i/\lambda_z = 1.70$ case we have for the $z_i/\lambda_z = 1.85$ case the same long time adjustment which includes a *second* level of self-induced wave resonance.

It should be clear from the above discussion of the drag histories shown in Fig. 4 that our results do very strongly support the existence of a nonlinear resonance in the field of internal waves and that this critical level resonance exists only when z_i/λ_z is near $\frac{3}{4} + n$ as we had hoped might be the case. This idea is strongly reinforced by the presentation of the data in Fig. 5 for which we have plotted the wave drag in the model at the end of the simulation, along with an estimate of its variance, as a function of the nondimensional critical layer height z_i/λ_z. There clearly are rather well defined resonant peaks near $z_i/\lambda_z = 0.75$ and $z_i/\lambda_z = 1.75$. The dashed line on Fig. 5 is the surface wave drag that would be predicted by Long's model for a flow with a height independent wind speed of -8 m s^{-1}. Clearly when the system is on resonance and the direct and reflected waves are interfering constructively the response is very much in excess of that predicted by Long's model. It is also interesting to note that the factor by which the wave drag exceeds that predicted by Long's model is the same factor (between 2 and 3) by which the drag was shown to increase in the breaking wave simulation described in Section 2. It is clear that the same physical process is at work in both of these internal wave dominated flows. When the system is off resonance the results in Fig. 5 show the expected decrease in the surface drag below the prediction of Long's model due to the destructive interference between the direct and reflected waves which characterizes these geometric conditions.

Figure 6 illustrates the evolution of the Reynolds stress profile for on-resonance and off-resonance flows using for illustrative purposes those for $z_i/\lambda_z = 0.75$, 1.15, and 1.75. In each of these cases the momentum flux in the wave field drops to zero above the critical level, implying the absence of any significant transmission of internal waves through this level. For the flows which are on-resonance the Reynolds stress also

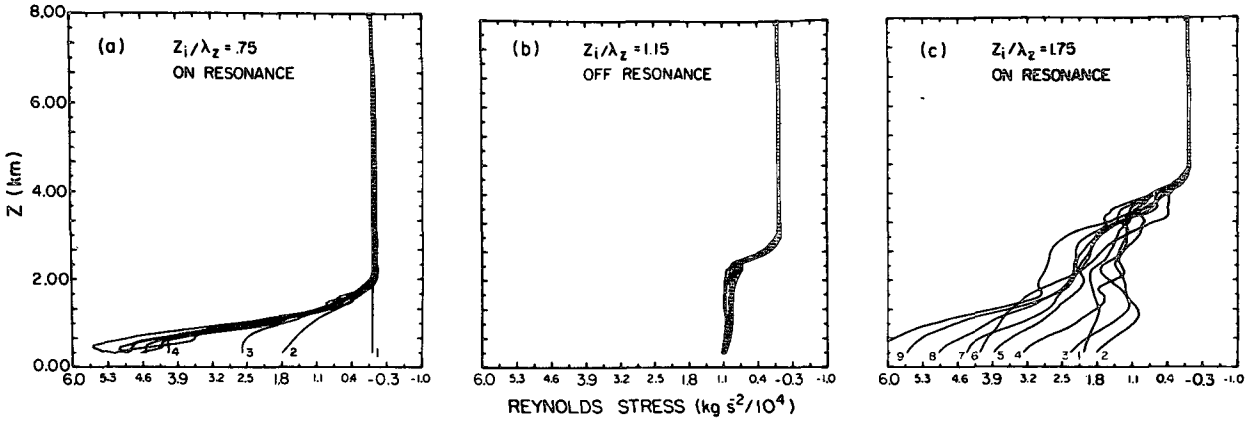

FIG. 6. Evolution of the Reynolds stress profile for on-resonance flows with $z_i/\lambda_z = 0.75$ and 1.75 and for the off-resonance flow with $z_i/\lambda_z = 1.15$. The profiles in the figure range in time from 0 to $2880\Delta t$, 1440 to $2880\Delta t$, and 2080 to $4240\Delta t$ for plates (a) to (c), respectively. Some of the profiles are sequentially numbered from earliest to latest. Note the strong divergence of the low level stress profiles which develop in the on-resonance cases compared with the nondivergent profile which characterizes the off-resonance case.

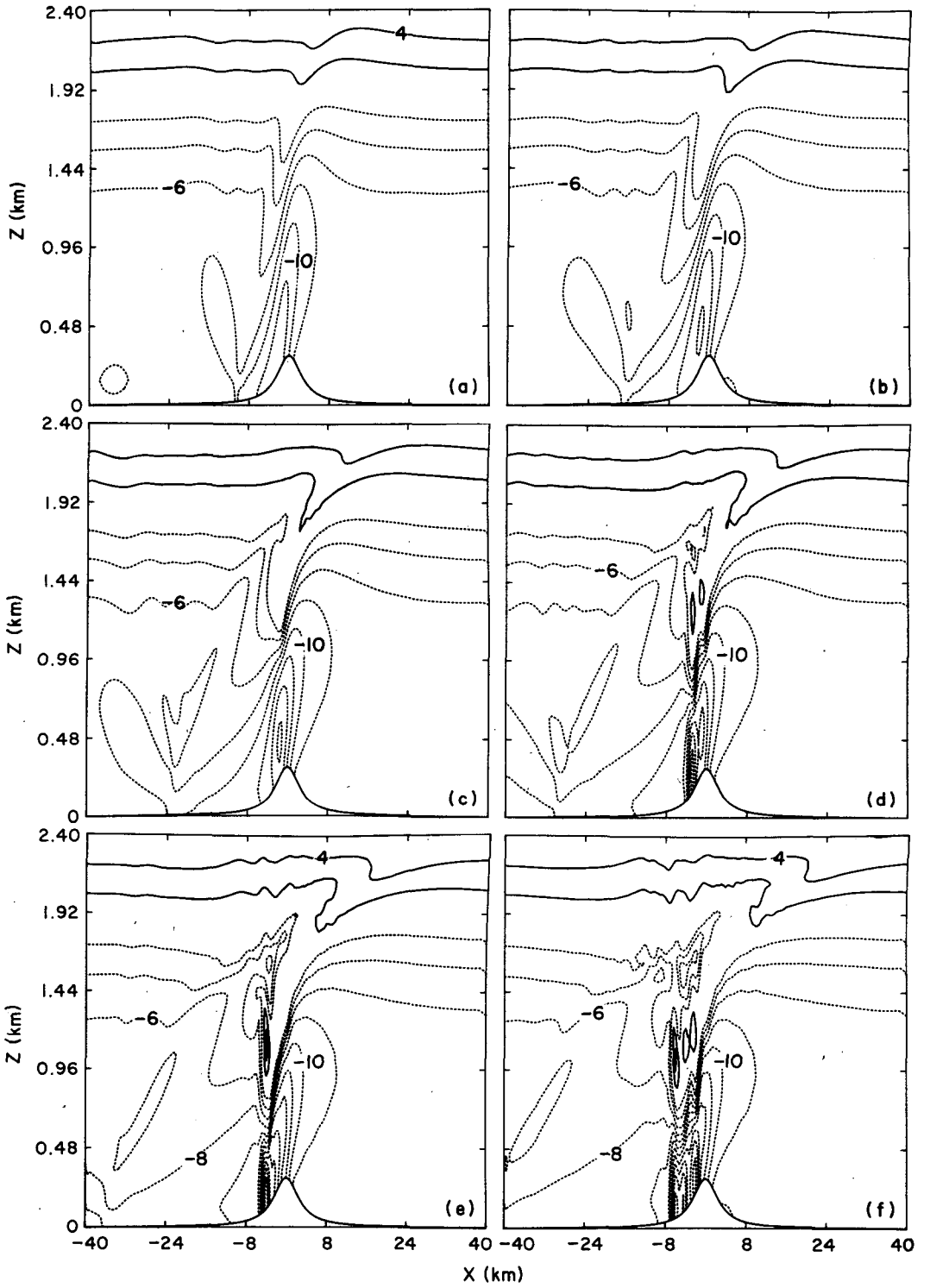

FIG. 7. Sequence of time slices through the evolving horizontal velocity field for the flow with $z_i/\lambda_z = 0.75$. The times shown are (a) 1200 s, (b) 2000 s, (c) 2800 s, (d) 3600 s, (e) 4400 s, (f) 5200 s. The contour interval is 2.00 m s^{-1}. Positive values are indicated by solid contours and negative values by dashed contours. The zero contour is not shown. The plot shows only a portion of the vertical domain whereas the full domain height is 8 km in all experiments. Note the stagnant tongue of fluid protruding down from the critical level which develops in this on-resonance case.

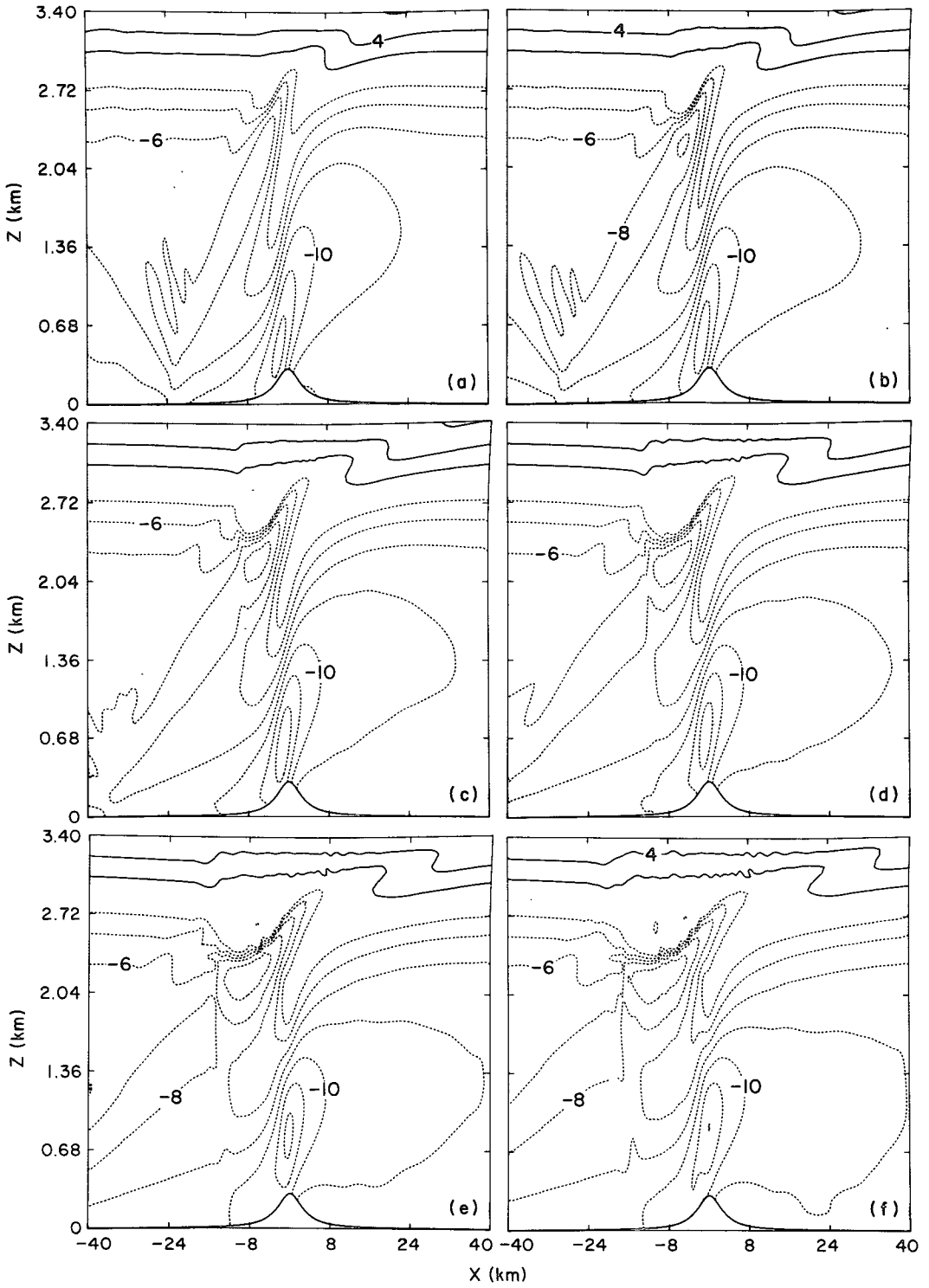

FIG. 8. As in Fig. 7 but $z_i/\lambda_z = 1.15$ and the times shown are (a) 2800 s, (b) 3600 s, (c) 4400 s, (d) 5200 s, (e) 6000 s, (f) 6800 s. Note that in this off-resonance case the stagnant tongue of fluid observed in Fig. 7 does not develop. Rather two relatively stagnant but shallow deformations of the critical surface form upstream and downstream of the mountain peak.

diverges strongly as a function of time in the low levels just as was found to be the case for the breaking wave simulations described in Section 2. If the topographic forcing in the calculations was horizontally sinusoidal then the strong vertical divergence of the momentum flux across the critical level obtained in

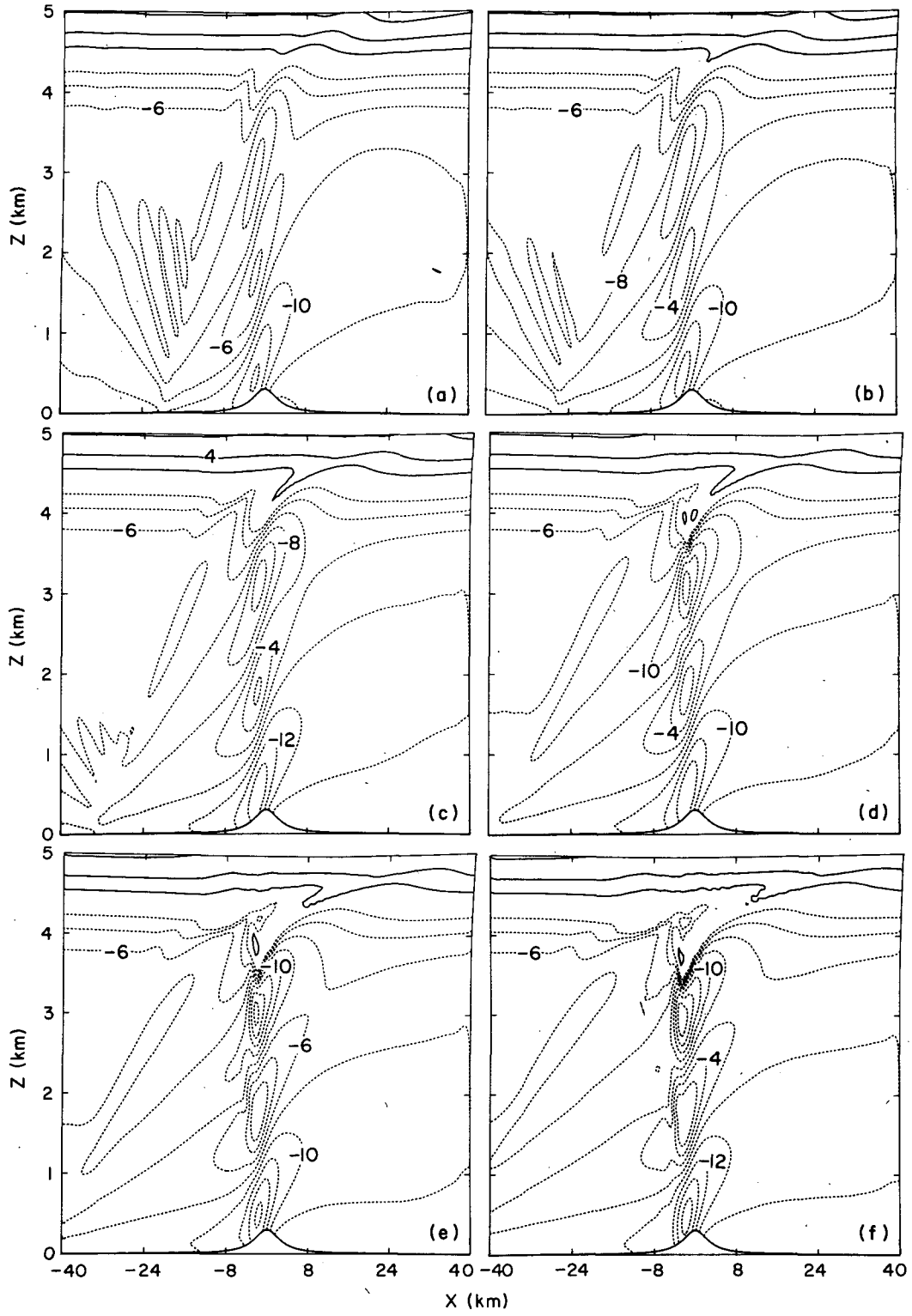

FIG. 9. As in Fig. 7 and 8 but for $z_i/\lambda_z = 1.75$ and the times shown are (a) 2400 s, (b) 3200 s, (c) 4000 s, (d) 4800 s, (e) 5600 s, (f) 6400 s. Note that in this on-resonance case the stagnant tongue of fluid again appears as in Fig. 7.

each of these calculations would be taken to imply a marked wave induced modification of the mean flow in this region. It is important to keep in mind that in the present circumstances, in which the upstream boundary conditions are maintained, no such irreversible modification of the mean flow need be implied

by the observed stress drop and no significant mean flow modification is in fact obtained. This is because the nonlinear interaction of the wave field with the mean flow at the critical layer is such that no significant absorption takes place although linear theory suggests that this should be the dominant process. Rather than being absorbed, the incident waves are simply reflected.

There is one additional feature of the on-resonance, off-resonance flows which does warrant some detailed discussion. This concerns the nature of the flow which develops in the critical layer itself under these different conditions. Figures 7, 8, and 9 each show a sequence of snapshots of the total horizontal velocity field for the simulations with $z_i/\lambda_z = 0.75$ (on-resonance), 1.15 (off-resonance), and 1.75 (on resonance) with the specific times in each case equally spaced and spanning the later stages of evolution. Intercomparison of these three sets of plates shows that the nature of the flow which develops near the critical level is strikingly different when the system is on-resonance compared to when it is off-resonance. In each of the on-resonance cases a tongue of stagnant fluid develops in the critical layer immediately overhead of the topography and protrudes into the underlying fluid. The depth to which this region extends increases as the surface drag increases. In the off-resonance case this feature is entirely absent. Rather, the flow in the critical level contains *two* regions in which the fluid is relatively stagnant, one upstream of the topographic maximum and the other downstream. As the system moves closer to resonance these two stagnant regions merge to produce the single deep stagnant tongue of fluid which is characteristic of the flow in the critical layer itself in the resonant state. Although these regions have some features in common with the analysis of the nonlinear mountain wave critical layer interaction presented by Marjolis and Su (1978), that analysis was rather inconclusive since it was based upon an *a priori* assumption of steady state behavior and it proved impossible to obtain analytically consistent results in the context of this assumption.

Our reason for drawing attention to this feature of the wave mean flow interaction at the critical layer is because precisely the same feature has previously been shown to be characteristic of the flows induced by wave breaking in circumstances in which strong downslope windstorms occur. The detailed analysis by Peltier and Clark (1979) of the strong downslope windstorm which occurred on 11 January 1972 in Boulder, Colorado showed that when our numerical model was initialized with upstream profiles of wind and stability it very accurately predicted the flow observed over the front range topography using instrumented aircraft. Figure 10 reproduces the isentrope and total horizontal velocity fields predicted by the numerical model after an integration time of about 2 hours. These fields agree very well with the observations of this event reported by Lilly and Zipser (1972) (e.g., see Lilly, 1978). The physical process which leads to the large amplitude wave observed and predicted by the model is the same breaking wave process of low level resonant amplification discussed in the context of simpler basic state flows in Section 2. This interaction inevitably produces a deep stagnant tongue of air in the region where the

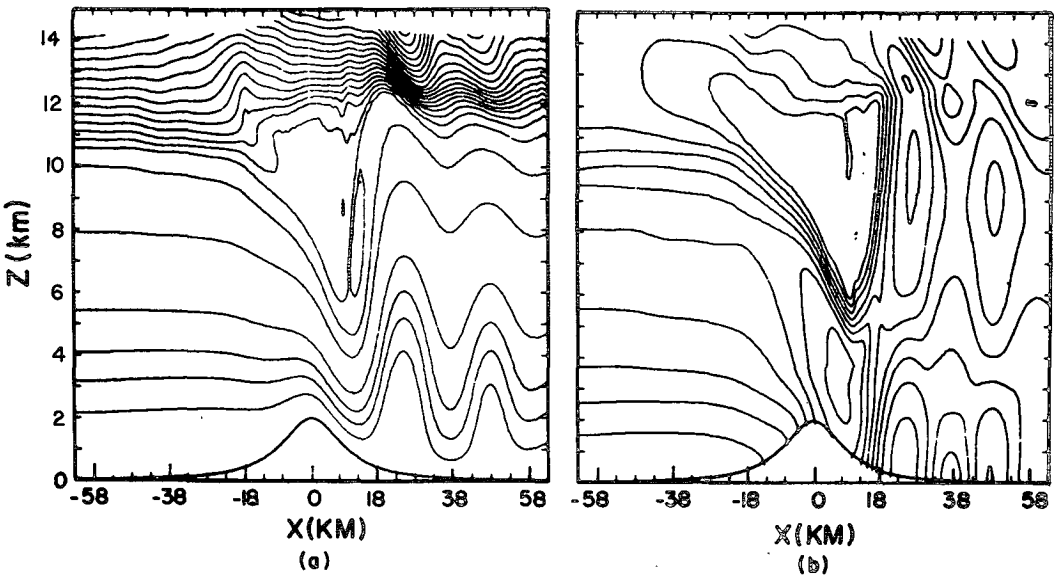

FIG. 10. Isentrope (a) and total horizontal velocity field (b) produced by the numerical simulation of Peltier and Clark (1979) of the severe downslope windstorm observed at Boulder, Colorado on 11 January 1972. Note the vertically oriented deep stagnant tongue of fluid which develops in the region where the wave breaks in the lower stratosphere and which then grows downward as the flow develops.

streamlines are held vertical—see the fields in Fig. 10. Precisely the same feature has now been shown to characterize the evolution of the wave field in mean flows with critical layers when the distance of the critical level above the ground is such that the internal wave cavity is resonant. This is further strong qualitative support for our resonant amplification hypothesis as to the physical mechanism which supports the increase of wave intensity in the low levels following breaking.

5. Conclusions

These analyses of the interaction of a forced packet of internal waves with the mean flow at a critical layer have established several interesting new results. First, when the critical level is one at which the local gradient Richardson number is significantly greater than 0.25 the nonlinear interactions are such that no significant absorption of wave momentum occurs in flows forced by localized topography. Rather, the internal waves are quite strongly reflected. Secondly, when such a critical level is located at a height $z = 3\lambda_z/4$ (or $n\lambda_z$ in excess of this) above the level of forcing, the direct and reflected waves interfere constructively and an intense resonant growth of the low-level wave field ensues. The observed resonance is one which has a fairly broad peak so that one may be 10%, or so, removed from the precise quantization condition and still obtain strong wave amplification.

The demonstration that the wave guide is resonant only if its vertical extent is near $3\lambda_z/4$ (or some $n\lambda_z$ is excess of this) provides strong support for our previous interpretation of the low-level wave amplification observed in breaking wave simulations. Since we have previously established that the wave amplification which occurs subsequent to breaking is required to understand observations of severe downslope windstorm occurrence, it is clear that the resonant amplification process is rather fundamental to the dynamics of such naturally occurring flows. Even though the final characteristics of such flows do bear a strong qualitative resemblance to those associated with hydraulic jumps, the mechanism of wave trapping effected at the level of supercritically steepened streamlines is clearly crucial to understanding how these flows evolve into the final states which are observed in nature.

Acknowledgments. This research was supported in part by NSERC Grant A-9627. The numerical computations were performed on the CRAY-1 computer at the National Center for Atmospheric Research, which is supported by the National Science Foundation.

REFERENCES

Béland, M., and T. Warn, 1975: The radiation condition for transient Rossby waves. *J. Atmos. Sci.*, **32**, 1873–1880.

Booker, J. R., and F. P. Bretherton, 1967: The critical layer for internal gravity waves in a shear flow. *J. Fluid Mech.*, **27**, 513–539.

Clark, T. L., 1977: A small scale numerical model using a terrain following co-ordinate system. *J. Comput. Phys.*, **24**, 186–215.

——, and W. R. Peltier, 1977: On the evolution and stability of finite amplitude mountain waves. *J. Atmos. Sci.*, **34**, 1715–1730.

——, and R. D. Farley, 1984: Severe downslope windstorm calculations in two and three spatial dimensions using interactive grid nesting: A possible mechanism for gustiness. *J. Atmos. Sci.*, **41**, 329–350.

Davis, P. A., and W. R. Peltier, 1976: Resonant parallel shear instability in the stably stratified planetary boundary layer. *J. Atmos. Sci.*, **33**, 1287–1300.

——, and ——, 1977: Effects of dissipation upon parallel shear instability near the ground. *J. Atmos. Sci.*, **34**, 1868–1884.

——, and ——, 1979: Some characteristics of the Kelvin-Helmholtz and resonant over-reflection modes of shear flow instability and of their interaction through vortex paving. *J. Atmos. Sci.*, **36**, 2394–2412.

Klemp, J. B., and D. R. Duran, 1983: An upper boundary condition permitting internal gravity wave radiation in numerical mesoscale models. *Mon. Wea. Rev.*, **111**, 430–444.

Koop, C. G., 1981: A preliminary investigation of the interaction of internal gravity waves with a steady shearing motion. *J. Fluid Mech.*, **113**, 347–386.

Lilly, D. K., 1962: On the numerical simulation of buoyant convection. *Tellus*, **14**, 148–172.

——, 1978: A severe downslope windstorm and aircraft turbulence induced by a mountain wave. *J. Atmos. Sci.*, **35**, 59–77.

——, and J. B. Klemp, 1980: Comments on "The evolution and stability of finite-amplitude mountain waves. Part II: Surface wave drag and severe downslope windstorms." *J. Atmos. Sci.*, **37**, 2119–2121.

——, and E. J. Zipser, 1972: The front range windstorm of 11 January 1972—A meteorological narrative. *Weatherwise*, **25**, 56–63.

Long, R. R., 1953: Some aspects of the flow of stratified fluids. 1. A theoretical investigation. *Tellus*, **5**, 42–58.

Margolis, S. B., and C. H. Su, 1978: Boundary-value problems in stratified shear flows with a nonlinear critical layer. *Phys. Fluids*, **21**, 1247–1259.

Miles, J. W., 1961: On the stability of heterogeneous shear flows. *J. Fluid Mech.*, **10**, 496–508.

——, and H. E. Huppert, 1969: Lee waves in a stratified flow. Part IV: Perturbation approximations. *J. Fluid Mech.*, **35**, 497–525.

Orlanski, I., 1976: A simple boundary condition for unbounded hyperbolic flows. *J. Comput. Phys.*, **21**, 251–269.

Peltier, W. R., and T. L. Clark, 1979: The evolution and stability of finite-amplitude mountain waves. Part II: Surface wave drag and severe downslope windstorms. *J. Atmos. Sci.*, **36**, 1498–1529.

——, and ——, 1980: Reply to comments of D. K. Lilly and J. B. Klemp on "The evolution and stability of finite amplitude mountain waves." Part II: Surface wave drag and severe downslope windstorms. *J. Atmos. Sci.*, **37**, 2122–2125.

——, and ——, 1983: Nonlinear mountain waves in two and three spatial dimensions. *Quart. J. Roy. Meteor. Soc.*, **109**, 527–548.

Warn, T., and H. Warn, 1978: The evolution of a nonlinear Rossby wave critical level. *Stud. Appl. Math.*, **59**, 37–71.